Molecular Recognition of Macrocyclic Peptidomimetic Inhibitors by HIV-1 Protease[†,‡]

Jennifer L. Martin,* Jake Begun,[§] Aaron Schindeler,[||] Wasa A. Wickramasinghe,[⊥] Dianne Alewood, Paul F. Alewood, Douglas A. Bergman, Ross I. Brinkworth, Giovanni Abbenante, Darren R. March,[@] Robert C. Reid, and David P. Fairlie

Centre for Drug Design and Development, University of Queensland, Brisbane QLD 4072, Australia

Received January 25, 1999; Revised Manuscript Received April 8, 1999

ABSTRACT: High-resolution crystal structures are described for seven macrocycles complexed with HIV-1 protease (HIVPR). The macrocycles possess two amides and an aromatic group within 15−17 membered rings designed to replace N- or C-terminal tripeptides from peptidic inhibitors of HIVPR. Appended to each macrocycle is a transition state isostere and either an acyclic peptide, nonpeptide, or another macrocycle. These cyclic analogues are potent inhibitors of HIVPR, and the crystal structures show them to be structural mimics of acyclic peptides, binding in the active site of HIVPR via the same interactions. Each macrocycle is restrained to adopt a β-strand conformation which is preorganized for protease binding. An unusual feature of the binding of C-terminal macrocyclic inhibitors is the interaction between a positively charged secondary amine and a catalytic aspartate of HIVPR. A bicyclic inhibitor binds similarly through its secondary amine that lies between its component N-terminal and C-terminal macrocycles. In contrast, the corresponding tertiary amine of the N-terminal macrocycles does not interact with the catalytic aspartates. The amine−aspartate interaction induces a 1.5 Å N-terminal translation of the inhibitors in the active site and is accompanied by weakened interactions with a water molecule that bridges the ligand to the enzyme, as well as static disorder in enzyme flap residues. This flexibility may facilitate peptide cleavage and product dissociation during catalysis. Proteases [Aba^{67,95}]HIVPR and [Lys^{7},Ile^{33},Aba^{67,95}]-HIVPR used in this work were shown to have very similar crystal structures.

Human immunodeficiency virus type-1 (HIV-1)[1] is the causative agent of acquired immunodeficiency syndrome (AIDS). Since the aspartyl protease enzyme from HIV-1 (HIVPR) is essential for viral replication, it is a target for therapeutic intervention in the disease (*1*−*3*). The enzyme processes viral proteins from precursors encoded by the *gag* and *gag-pol* HIV genes, and its inhibition has been shown to prevent viral maturation and the production of infectious progeny virus (*4*−*6*).

The crystal structure of the uncomplexed form of HIVPR was determined in 1989 (*7*, *8*). The first cocrystal structure of an HIVPR−inhibitor complex was also reported in 1989 (*9*). Since then, the structures of many HIVPR−inhibitor complexes have been determined (for reviews, see refs *10*−*12*). Structures of HIVPR complexes have been deposited in the Protein Data Bank (PDB) (*13*), and more recently, the HIV protease database was established (*14*) (http://www-fbsc.ncifcrf.gov/HIVdb) as a repository for structures of HIVPR−inhibitor complexes.

Computer modeling based on crystal structures of known HIVPR−peptide inhibitor complexes suggests that the enzyme can accommodate cyclized tripeptide analogues corresponding to the linear sequences of peptidomimetic inhibitors. Inhibitors designed in this way would have the advantage of being conformationally restrained and preorganized for protease binding, binding with reduced entropy. In addition, the cyclic inhibitors are more resistant to proteolytic degradation than linear peptidomimetic inhibitors (*15*). Furthermore, these constrained macrocycle templates can be used to independently optimize inhibitor components. Macrocycles corresponding to both the N- and C-termini of HIVPR inhibitors have been synthesized and are potent inhibitors of HIVPR (*16*, *17*).

Here we describe the crystal structures of complexes formed between HIVPR and seven macrocycles that each inhibit the enzyme at nanomolar concentrations (Chart 1). Four of these inhibitors contain macrocycles as mimics for

[†] This work was supported by an ARC Queen Elizabeth II Fellowship to J.L.M. and NHMRC Grant 33190 to D.P.F.

[‡] Coordinates deposited under PDB file names 1b6j, 1b6k, 1b6l, 1b6m, 1b6n, 1b6o, and 1b6p.

* To whom correspondence should be addressed. Telephone: +61 7 3365 4942. Fax: +61 7 3365 1990. E-mail: j.martin@mailbox.uq.edu.au.

[§] Present address: Health Science and Technology Program, Harvard Medical School, 270 Longwood Ave., Boston, MA 02115.

[||] Present address: Victor Chang Cardiac Research Institute, 384 Victoria St., Darlinghurst NSW 2010, Australia.

[⊥] Present address: National Research Centre for Environmental Toxicology, 39 Kessels Rd., Coopers Plains QLD 4108, Australia.

[@] Present address: Research School of Chemistry, Australian National University, Canberra ACT 2600 Australia.

[1] Abbreviations: Aba, L-α-amino-*n*-butyric acid; DMSO, dimethyl sulfoxide; HIV, human immunodeficiency virus; HIVPR, chemically synthesized protease enzyme from HIV-1 (SF2 isolate) with Cys67 and Cys95 replaced with Aba ([Aba^{67,95}]HIVPR); HIVKI, as described for HIVPR but with two additional sequence changes (Gln7Lys and Leu33Ile) to limit autoproteolysis ([Lys^{7},Ile^{33},Aba^{67,95}]HIVPR); rmsd, root-mean-square deviation; RP-HPLC, reversed phase high-pressure liquid chromatography.

10.1021/bi990174x CCC: $18.00
Published on Web 06/22/1999

Chart 1: Structures of Macrocyclic Peptidomimetic Inhibitors of HIV-1 Protease

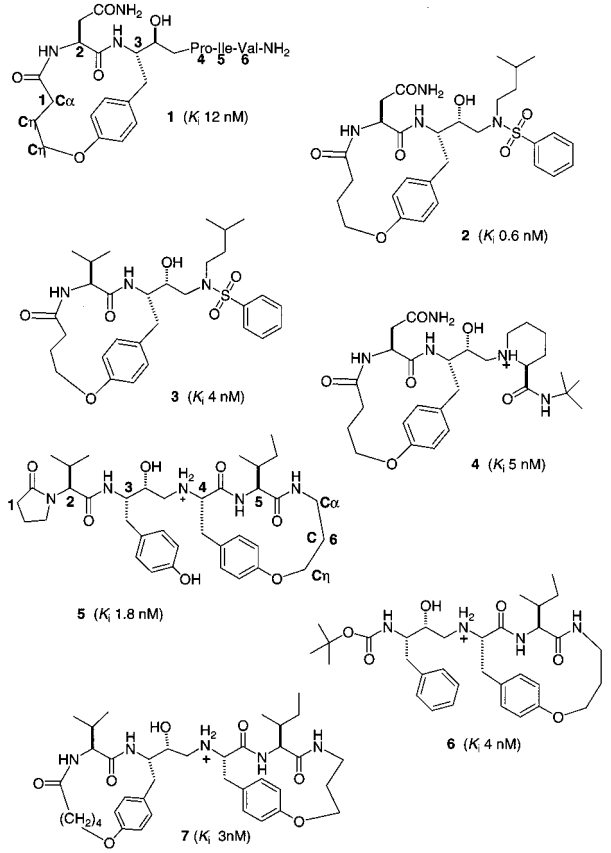

N-terminal tripeptide sequences. Two inhibitors have a macrocycle which replaces a C-terminal tripeptide, and one compound connects both N- and C-terminal macrocycles via a hydroxyethylamine transition state isostere to form a bicyclic surrogate for a hexapeptide sequence. The seven high-resolution crystal structures reveal the molecular basis for the effectiveness of using such macrocyclic peptidomimetics as components of protease inhibitors and show that most interactions made by peptides with HIVPR are reproduced by the macrocyclic analogues.

EXPERIMENTAL PROCEDURES

Inhibitor and Protein Synthesis and Preparation. Synthesis of the macrocyclic peptidomimetic inhibitors was carried out as described previously (*15*−*17*). [Aba^{67,95}]HIVPR (SF2 isolate) and [Aba^{67,95}]HIVKI were chemically synthesized in our laboratories by solid phase peptide synthesis (*18*, *19*). The two cysteine residues (Cys67 and Cys95) of the native sequence were replaced with the isosteric analogue L-α-amino-*n*-butyric acid (Aba) for ease of synthesis and handling to yield [Aba^{67,95}]HIVPR (*7*). This enzyme was fully active and had the same kinetic properties as the cloned enzyme (*19*). [Aba^{67,95}]HIVPR, which we refer to as HIVPR, was used in the HIVPR−**1** cocrystallization experiment. For all other cocrystallizations, there were two additional changes to the sequence at autocleavage sites (Q7K and L33I) to limit autolysis (*20*, *21*). This gave the enzyme [Lys^{7},Ile^{33},Aba^{67,95}]-HIVPR which we refer to as HIVKI. This enzyme retained biochemical activity and had kinetics similar to those of both synthetic HIVPR and recombinant HIVPR (HXB2 isolate); K_m values for substrate are 46 (HIVKI), 21 (synthetic HIVPR), and 45 μM [recombinant HIVPR (HXB2 isolate)] (D. A. Bergman, unpublished). Details of comparative kinetics will be published elsewhere.

For preparation of the enzyme for crystallization, we followed the method described by Hui et al. (*22*) for purifying and refolding expressed HIVPR from inclusion bodies. The lyophilized synthetic protein was dissolved in 50% acetic acid to a concentration of 1.5 mg/mL and then diluted into 25 volumes of 0.1 M acetate buffer (pH 5.5), 5% ethylene glycol, and 10% glycerol. The diluted enzyme solution was exchanged into the crystallization buffer [0.1 M acetate buffer (pH 5.5)] and the protein concentrated to 5 mg/mL using Centriprep-10 and Centricon-10 ultrafiltration devices (Amicon) over a period of 8 h. This method was used for all enzyme preparations except that used for the HIVPR−**1** complex, in which the guanidine refolding and dialysis method described by Wlodawer et al. (*7*) was used.

HIVPR Inhibition Assay. Enzyme activity was measured using a continuous fluorimetric assay described previously (*19*, *23*). Inhibition of HIVPR was assessed using the following conditions: 37 °C, 100 mM MES buffer at pH 6.5 [containing 10% (v/v) glycerol and 50 μg/mL bovine serum albumin], and 50 μM substrate [2-(aminobenzoyl)-Thr-Ile-Nle-Phe(*p*-NO_2)-Gln-Arg-NH_2]. The amino acid content of inhibitors was quantified, after decomposition (6 N HCl for 24 h at 110 °C) and derivitization, by RP-HPLC with norleucine as the internal standard.

Crystallization. Inhibitors were dissolved in DMSO at a concentration of 50−150 mM, depending on the solubility. The purified and concentrated HIVPR or HIVKI (5 mg/mL) in 0.1 M acetate buffer (pH 5.5) was mixed with inhibitor in a volume ratio of 10:1, and left on ice for at least 30 min prior to crystallization. The final concentrations were ∼5 mg/mL HIVPR (or HIVKI) and 5−15 mM inhibitor.

Crystallization was achieved by the method of hanging drop vapor diffusion. The enzyme/inhibitor solution was mixed in a 1:1 ratio with precipitant solution, with final volumes varying from 1 to 5 μL. One milliliter of the precipitant, consisting of 30−60% ammonium sulfate and 0.1 M acetate buffer (pH 5.4−5.6), was placed in the reservoir. Rod-shaped crystals appeared in the hanging drop within 7−10 days and continued to grow over the following 7 days. Crystals used for data collection varied in size from 0.05 mm × 0.05 mm × 0.4 mm (for the HIVPR−**3** cocrystal) to 0.2 mm × 0.2 mm × 0.5 mm (for the HIVPR−**1** cocrystal). The average crystal size was 0.1 mm × 0.1 mm × 0.2 mm.

Data Collection and Data Processing. Crystallographic diffraction data were measured at 16 °C using an RAXIS-IIC imaging plate area detector with an RU-200 rotating anode generator. For the HIVPR−**1** cocrystal, a graphite monochromator was used, the crystal−detector distance was 100 mm, and the oscillation range was 3°. For all other cocrystals, a Yale mirror monochromator with a Ni filter was used, the crystal−detector distance was 75 mm (except in the case of the cocrystal with HIVPR−**3**, where it was 82 mm), and the oscillation range was 2°. Frames were integrated, scaled, and merged using Denzo and Scalepack (*24*).

HIVPR or HIVKI crystals diffract to 2 Å or better and are isomorphous with previously described cocrystals of synthetic HIVPR and inhibitor (*9*, *25*). They belong to space

Table 1: Statistics for Crystallographic Data Measurement

	HIVPR−**1**	HIVKI−**2**	HIVKI−**3**	HIVKI−**4**	HIVKI−**5**	HIVKI−**6**	HIVKI−**7**
resolution (Å)	1.85	1.85	1.80	1.75	1.85	1.76	2.0
no. of observed reflections ($I/\sigma I > 1$)	84427	35422	35879	54139	45805	52836	27045
no. of unique reflections	14847	14904	15458	17359	15429	17002	11387
R_{sym}[a] (top shell)[b]	0.066 (0.230)	0.073 (0.295)	0.064 (0.293)	0.079 (0.272)	0.065 (0.276)	0.046 (0.276)	0.090 (0.216)
completeness (%) (top shell)[b]	89.1 (50.4)	89.8 (76.5)	84.6 (66.2)	88.1 (75.9)	91.5 (80.8)	87.5 (71.2)	85.6 (81.0)
$I/\sigma I$ (top shell)[b]	12.5 (3.9)	9.8 (2.2)	10.4 (2.2)	9.6 (2.5)	10.7 (2.7)	12.3 (2.7)	8.7 (3.5)
mosaicity (deg)	0.25	0.55	0.45	0.3	0.52	0.42	0.20

[a] $R_{sym} = \Sigma_h(I_h - \langle I_h\rangle)/\Sigma\langle I_h\rangle$. [b] The top shell is the highest-resolution shell for each data set. For HIVPR−**1** it is 1.92−1.85 Å, for HIVKI−**2** 1.92−1.85 Å, for HIVKI−**3** 1.86−1.80 Å, for HIVKI−**4** 1.81−1.75 Å, for HIVKI−**5** 1.92−1.85 Å, for HIVKI−**6** 1.82−1.76 Å, and for HIVKI−**7** 2.07−2.00 Å.

Table 2: Crystallographic Refinement Statistics

	1	**2**	**3**	**4**	**5**	**6**	**7**
resolution range (Å)	8−1.85	8−1.85	8−1.85	8−1.75	8−1.85	8−1.85	8−2.0
no. of protein atoms	1529[a]	1512[a]	1581[a]	1560[a]	1515[a]	1556[a]	1525[a]
no. of inhibitor atoms	49	46[a]	45[a]	39	49	43	52[a]
no. of water atoms	120	102	115	99	95	95	99[a]
no. of sulfate atoms	3 × 5	3 × 5	3 × 5	3 × 5	3 × 5	3 × 5	3 × 5
no. of reflections ($F > 0\sigma F$)	14540	14672	14204	17014	15126	14777	11099
R-factor[b] (top shell)[c]	0.175 (0.231)	0.193 (0.287)	0.192 (0.287)	0.202 (0.306)	0.209 (0.292)	0.195 (0.282)	0.185 (0.234)
R-free[d] (top shell)[c]	0.219 (0.246)	0.223 (0.260)	0.244 (0.308)	0.226 (0.301)	0.239 (0.312)	0.227 (0.262)	0.240 (0.286)
rmsd from ideal							
bond lengths (Å)	0.006	0.006	0.007	0.006	0.006	0.005	0.005
bond angles (deg)	1.4	1.3	1.3	1.3	1.3	1.2	1.3
dihedral angles (deg)	27.1	27.2	27.0	26.7	27.0	27.0	26.8
improper angles (deg)	1.48	1.13	1.29	1.21	1.16	1.15	1.15
Ramachandran statistics							
% in most favored region	95.5	96.8	95.5	94.2	96.8	97.4	95.5
% in disallowed region	0	0	0	0	0	0	0
coordinate error (Å)[e]	0.18−0.21	0.19−0.22	0.20−0.24	0.20−0.23	0.21−0.24	0.20−0.22	0.20−0.27
$\langle B\rangle$ for all atoms (Å^2)[f]	19.4	18.0	21.4	20.8	16.8	22.7	17.6
$\langle B\rangle$ for inhibitor atoms (Å^2)[f]	18.4	13.6	19.6	17.3	13.1	20.3	18.2

[a] Including alternative conformations. [b] $R = \Sigma|F_o - F_c|/\Sigma F_o$. [c] The top shell is the highest-resolution shell for each data set. For HIVPR−**1**, HIVKI−**2**, HIVKI−**3**, HIVKI−**5**, HIVKI−**6** it is 1.96−1.85 Å, for HIVKI−**4** 1.86−1.75 Å, and for HIVKI−**7** 2.12−2.00 Å. [d] Cross validation *R*-factor using 5−10% of the data. [e] Coordinate error from Luzzati plot analysis (*41*). [f] $\langle B\rangle$ is the average *B*-factor.

group $P2_12_12_1$, with the following unit cell parameters: a = 51.2−51.8 Å, b = 58.8−59.2 Å, and c = 61.9−62.3 Å; there are two HIVPR (HIVKI) monomers (corresponding to the active homodimer) and one inhibitor molecule in the asymmetric unit. Statistics from data processing are given in Table 1.

Crystallographic Refinement. Initial phases for each of the cocrystal structures were obtained by difference Fourier synthesis using the structures of either the HIVPR−JG365 complex (PDB file name 7HVP) or the structure of the HIVPR−**1** complex (PDB file name 1CPI) as the starting model. Solvent and inhibitor atoms were removed from the models prior to the first round of refinement. Refinement was carried out using XPLOR 3.1 and later XPLOR 3.851 (*26*), and cross validation was performed with the use of the *R*-free values from 10% of the reflections (*27*) (5% of the reflections for HIVKI−**3**). First, simulated annealing molecular dynamics was performed using the standard X-PLOR protocol (temperature of 3000 K) to decouple *R* and *R*-free. Several rounds of X-PLOR refinement (positional and individual *B*-factor) and rebuilding using the graphics program O (*28*) were carried out on each of the structures. The parameters used for refinement were those of Engh and Huber (*29*). Water molecules were included if electron density was present at 3σ above the background in $F_o - F_c$ maps and 1σ above the background in $2F_o - F_c$ maps, and if at least one hydrogen bonding partner was found within a radius of 3.4 Å. Three sulfate ions (ammonium sulfate is used in the crystallization medium) were also identified and modeled in the structures. A low-resolution cutoff of 8.0 Å and structure factor amplitude cutoff of $0\sigma F$ were used. A high-resolution cutoff was also used in those cases where the highest-resolution shell had poor values for $F/\sigma F$ and *R*-free. Refinement statistics are given in Table 2.

Several residues on the surface of the enzyme are mobile in the crystal structures. These have been modeled as alanine, or with two alternate conformations, or with half-occupancy for side chain atoms. In some cases, enzyme main chain atoms (Ile50 and Gly51 in the flap region) and inhibitor atoms were modeled with alternative conformations (see the text for details).

Coordinates and structure factors of all seven protein crystal structures have been deposited with the Brookhaven Protein Data Bank (*13*) and the HIV Data Bank (*14*). PDB file names are as follows: 1b6j for HIVPR−**1** (replaces 1cpi), 1b6o for HIVKI−**2**, 1b6n for HIVKI−**3**, 1b6l for HIVKI−**4**, 1b6k for HIVKI−**5**, 1b6m for HIVKI−**6** (replaces 1mtr), and 1b6p for HIVKI−**7**.

Figures were generated using Setor (*30*), Molscript (*31*), and Raster3D (*32, 33*).

RESULTS

Chart 1 shows seven macrocyclic compounds (**1**−**7**) which we have previously designed and synthesized. They are all

potent inhibitors of HIV-1 protease with K_i values in the range of 0.6−12 nM. The enzyme (HIVPR) used for determining inhibition constants and for cocrystallization with inhibitor **1** was chemically synthesized with a sequence corresponding to the SF2 isolate with cysteines 67 and 95 replaced by isosteric L-α-amino-*n*-butyric acid as used in the original structural studies of HIVPR−inhibitor complexes (*7*, *9*, *25*). The enzyme used for cocrystallization with inhibitors **2**−**7** was also chemically synthesized, but with two additional mutations to limit autoproteolysis (see Experimental Procedures). Protein crystal structures for each of the seven inhibitors complexed with HIVPR were determined by difference Fourier analysis and refined to high resolution (Tables 1 and 2). All seven inhibitors bind in a single orientation in the active site substrate-binding groove of the homodimeric enzyme. A water molecule (Wat301) mediates interactions between backbone oxygens of the inhibitor and backbone nitrogens of enzyme flap residues Ile50 and Ile150.

An N-Terminal Macrocyclic Mimic for Leu-Asn-Phe. The macrocyclic inhibitor, **1**, was computer modeled into the active site of HIVPR (*16*) as a possible mimic of the heptapeptide inhibitor, JG365 (*25*). The acyclic JG365 has the sequence Ac-Ser-Leu-Asn-Phe-[(*S*)-CH(OH)CH_2]-Pro-Ile-Val-OCH_3 with a hydroxyethylamine isostere replacing the peptide scissile bond. Compound **1** incorporates a cyclic mimic of the N-terminal tripeptide Leu-Asn-Phe of JG365 (P1−P3) with the P4 N-terminal group (Ac-Ser) of JG365 removed. The isostere and C-terminal sequence (Pro4-Ile5-Val6) of JG365 are retained in **1**, albeit with a C-terminal amide rather than an ester. This shortened structural mimic of the acyclic JG365 imitates the function of JG365 by potently inhibiting HIVPR [for JG365, K_i = 1.8 nM (*19*); for **1**, K_i = 12 nM (*16*)].

A preliminary structure of the HIVPR−**1** complex has been communicated previously (*16*), but the more detailed structure reported here is improved with respect to both resolution (1.85 vs 2.0 Å) and the final crystallographic statistics. The quality of the electron density for **1** (and the other six macrocyclic inhibitors) is shown in Figure 1. The bound inhibitor is well-ordered, having an average *B*-factor similar to that of the enzyme (17−18 $Å^2$). The crystals used for structure determination of the enzyme complexes with both JG365 (*25*) and **1** were grown from the same form of synthetic enzyme ([$Aba^{67,95}$]HIVPR), allowing a direct comparison of the binding modes to be made. The enzyme structures in both complexes are very similar (rmsd of 0.34 Å for all 198 Cα atoms). The macrocyclic inhibitor **1** and JG365 bind to the enzyme in a very similar manner (Figure 2) via similar intermolecular hydrogen bonds (Figure 3). Hydrogen bonds between the enzyme and atoms of the Ac-Ser N-terminus of JG365 (which is not retained in **1**) are replaced with interactions with water molecules in the HIVPR−**1** complex. Differences that are observed between the HIVPR-bound conformations of JG365 and **1** are as follows.

The isostere hydroxyls of **1** and JG365 are separated by 0.6 Å; the hydroxyl of **1** is within hydrogen bonding distance (cutoff of 3.3 Å) of both carboxylate oxygens of Asp125, but only one of Asp25. Conversely, the hydroxyl of JG365 is within hydrogen bonding distance of both side chain oxygens of Asp25, but only one of Asp125 (Figure 3).

Table 3: Dihedral Angles of Isostere Rotatable Bonds

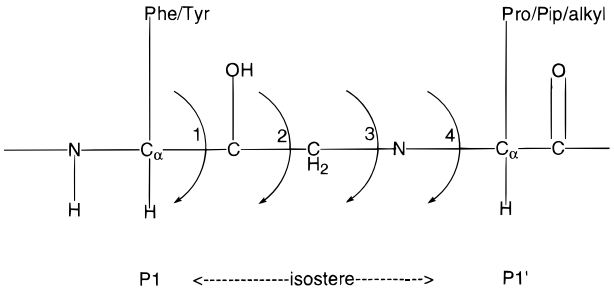

inhibitor complex	dihedral 1 (deg)	dihedral 2 (deg)	dihedral 3 (deg)	dihedral 4 (deg)
HIVPR−JG365	47	151	−12	−57
HIVPR−**1**	57	97	47	−98[a]
HIVPR−VX478	153	−59	94	84
HIVKI−**2**	179	−69	110	93
HIVKI−**3**	179	−71	110	97
HIVKI−**4**	170	−74	162	−61[a]
HIVKI−**5**	60	179	−134	63
HIVKI−**6**	60	178	−133	65
HIVKI−**7**	59	179	−133	58

[a] This dihedral angle is constrained in **1** and **4** because it represents the bond in a proline and piperidine cycle, respectively.

A hydrogen bond between the Ile5 backbone oxygen of **1** and the backbone nitrogen of HIVPR Asp129 is not observed in the HIVPR−JG365 complex (Figure 3).

The backbone dihedral angles of the P1−P1′ region of the two inhibitors vary (Table 3).

These apparent differences in binding mode between the macrocyclic and acyclic inhibitors probably result from the difference in resolution of the experimental data used for refinement (HIVPR−**1** determined at 1.85 Å and HIVPR−JG365 at 2.4 Å). However, one difference between the bound conformations that *is* due to the conformational constraints imposed by the macrocycle of **1** is the orientation of the inhibitor phenyl ring (Figure 2). The χ_1 dihedral angles of this aromatic residue differ by 25°. As a consequence, the hydrophobic contacts observed between the phenyl ring of JG365 and atoms from Gly49 and Ile50 are much weaker in the HIVPR−**1** complex, but interactions with Ile184 and Val182 are stronger than in the JG365 complex.

Atoms forming the macrocyclic link between the aromatic ring and Asn residue of **1** form the most flexible part of the inhibitor in the HIVPR−**1** complex. These atoms have reasonable electron density (Figure 1) but are less ordered than the rest of the inhibitor; the two central atoms in the macrocycle have *B*-factors of ∼26 $Å^2$. The crystal structure of HIVPR−**1** has a close contact between the macrocycle atom Cη_1 and the side chain Nη_2 of Arg108 (3.3 Å). This type of interaction is usually considered unfavorable, and so could contribute to the higher *B*-factor for this region of the bound inhibitor. However, a similar close contact (3.1 Å) is also observed in the HIVPR−JG365 complex between Arg108 Nη_2 and Leu Cδ_2 of JG365. In any event, we know that in solution this macrocycle is still quite constrained since the aromatic ring is not able to rotate at ambient temperature (*15*).

Comparison of [$Aba^{67,95}$]HIVPR and [Lys^7,Ile^{33},$Aba^{67,95}$]-HIVPR Structures. The macrocyclic inhibitors **2**−**7** were cocrystallized with HIVKI, which is modified at two

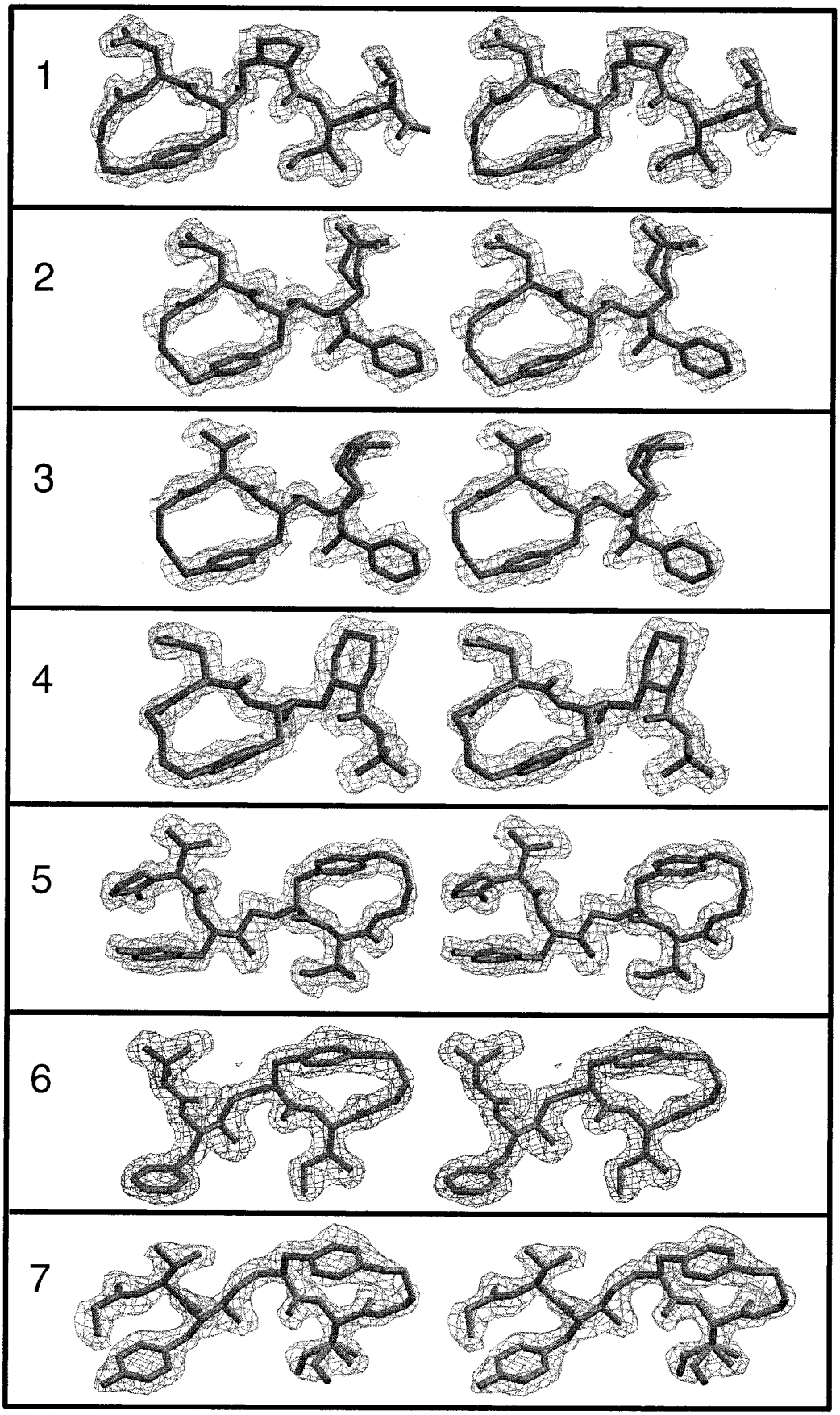

FIGURE 1: Stereoview of electron density for each of the seven inhibitors bound at the active site of HIVPR. The $2F_o - F_c$ maps are shown, calculated from the final refined structures and contoured at 1.2σ. For the bicycle, **7**, the density for a part of the N-terminal macrocycle (left-hand side of structure) is poor and two atoms in this macrocycle are not modeled.

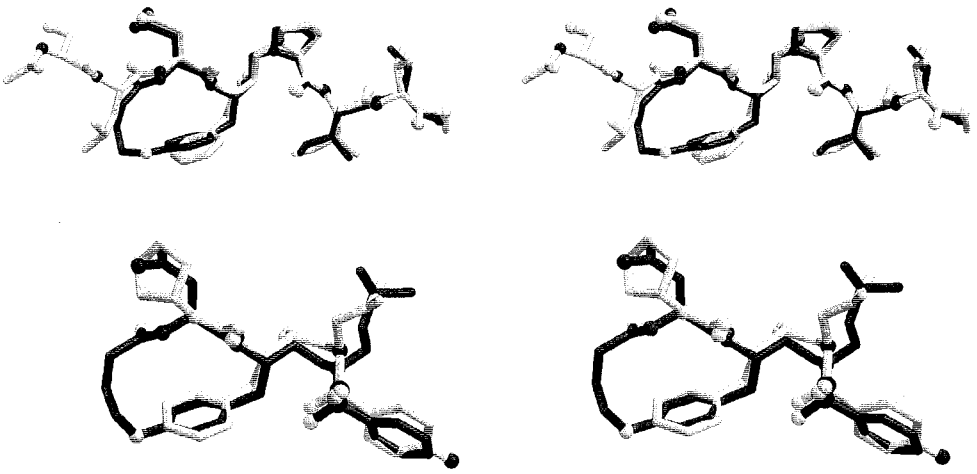

FIGURE 2: Stereodiagram showing (top) the comparison of the HIVPR-bound conformations of **1** (black) and JG365 (gray) and (bottom) the comparison of the HIVPR-bound conformations of **2** (black) and VX-478 (gray). The superimpositions are taken from the crystal structures of the HIVPR or HIVKI complexes, after alignment of the enzyme structures.

additional positions (Gln7Lys and Leu33Ile) compared with HIVPR (Aba67 and -95). These additional synthetic mutations to the enzyme sequence were made to limit autoproteolysis (*20*, *21*) and do not significantly change the kinetics (D. A. Bergman, private communication). The overall folds of HIVPR (as refined in the HIVPR−**1** complex) and HIVKI (as refined in the HIVKI−**2**−**7** complexes) are very similar with rmsds of 0.15−0.32 Å for all 198 residues of the homodimer. These rmsds are within the range of the estimated coordinate errors of the structures (Table 2). The local structure around the site of the two mutations is also very similar. Enzyme residue 7 is solvent-exposed and poorly ordered with the backbone being similar in all cases, but the side chain is flexible. In some of the structures described here, this residue was modeled with an alanine side chain or with a lysine side chain with half-occupancy. Where the lysine side chain was modeled, it had dihedral angles similar to those of the glutamine side chain in the HIVPR−**1** structure. Residue 33 is buried with its backbone and side chain conformations being similar for leucine or isoleucine. Overall, replacement of Gln7 with lysine and Leu33 with isoleucine in HIVPR produces no change in the local or global structure of the enzyme.

Stereoisomer Preference and Binding Conformation. The well-known effect of switching stereoisomer preference at the isostere chiral carbon of HIVPR inhibitors (*34*) is also observed for the macrocycle mimics. Thus, for **1** the (*S*)-diastereomer is the more potent inhibitor of HIVPR. When the proline P1′ residue of **1** is replaced with a larger hydrophobic group, such as the *N*-alkyl groups of **2** and **3**, the piperidine ring of **4**, or the phenyl rings of **5**−**7**, the stereoisomer preference switches from the (*S*)- to the (*R*)-diastereomer. This is because the larger hydrophobic groups at P1′ in the (*S*)-diastereomers cannot fit into the enzyme active site. The isomer preference therefore changes, with (*R*)-diastereomers making optimal interactions between the isosteric hydroxyl and catalytic aspartates through a conformational change centered around the transition state isostere (Table 3).

N-Terminal Macrocycles with a Nonpeptidic C-Terminus. Inhibitor **1** incorporates a macrocyclic analogue of the P1−P3 residues of JG365 with no changes in the C-terminal P1′−P3′ residues. We investigated the enzyme binding mode of

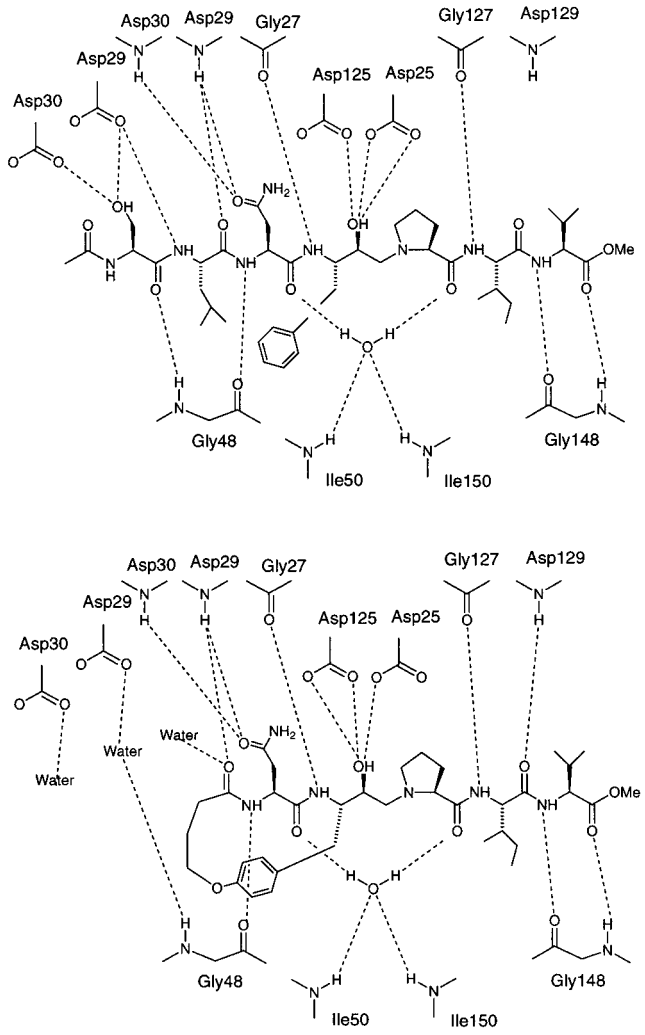

FIGURE 3: Hydrogen bond interactions with HIVPR for JG365 (top) and **1** (bottom). A 3.3 Å distance cutoff was used to define hydrogen bonds (dashed lines).

other N-terminal macrocyclic HIVPR inhibitors (**2**−**4**) in which alternative and shorter nonpeptidic groups replace the C-terminal tripeptide.

Compounds **2** and **3** incorporate the same N-terminal macrocycle as in **1**, although compound **3** has a valine rather than an asparagine side chain at P2. In both **2** and **3**, the

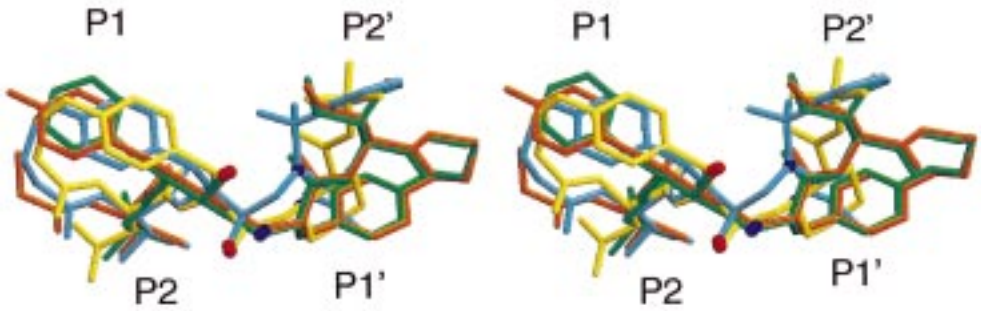

FIGURE 4: Stereodiagram showing the comparison of the bound positions of HIVPR−macrocyclic inhibitor complexes, after alignment of the HIVPR and HIVKI enzyme structures. The N-terminal macrocycle inhibitors, represented by **3** (blue), bind to the enzyme in a manner similar to that of the acyclic inhibitor JG365 (see Figure 2). Inhibitor **4** (yellow) is translated to the right (C-terminus) with respect to the other N-terminal macrocycle inhibitors, due to the bulky substituents at P1′ and P2′. The C-terminal macrocycles, represented by **6** (green), and the bicycle **7** (orange) are translated to the left (N-terminus) with respect to **1**−**4**, to enable interaction of the protonated secondary amine (dark blue sphere) with the catalytic aspartates. The P1 aromatic rings (top left) and the isostere hydroxyls (red spheres) are useful reference points for assessing the relative translations of the inhibitors in the HIVPR active site. Note that two atoms of the N-terminal macryocycle of **7** (orange) are disordered in the HIVPR complex (see Figure 1) so that the cyclic connection is not shown.

hydroxyethylamine isostere of **1** is retained, but the C-terminal tripeptide is replaced with a sulfonamide moiety similar to that used in the HIVPR inhibitor VX-478 (PDB file name 1HVP) (*35*). The sulfonamide groups of **2** and **3** are identical, but differ from that in VX-478 in that the *N*-alkyl group is lengthened by one methylene and the *p*-amino group of VX-478 is absent. The sulfonamide *N*-alkyl substituent corresponds to a P1′ side chain and the aromatic ring to a P2′ side chain of a conventional peptidic inhibitor of HIVPR. There is no P3′ equivalent to the valine of JG365 in compound **2** or **3**. Inhibitor **4** has the same N-terminal macrocycle (with Asn at P2) and scissile bond replaced with hydroxyethylamine isostere as in **1** and **2**. Compared with **1**, **4** has a piperidine rather than a proline at P1′ and a *tert*-butyl group in place of Ile at P2′. Although compounds **2**−**4** have no structural equivalent to the P3′ group, they are all more potent than the parent N-terminal macrocyclic compound **1** (Chart 1).

There is little difference between the structures of the proteins in the complexes with **1**−**3**, except that the observed side chain rotamer of Ile84 changes depending on whether Asn ($\chi_1 \sim 60°$) or Val ($\chi_1 \sim -60°$) is present at P2. This change in rotamer preference optimizes the van der Waals interaction between the hydrophobic P2 side chain and the Ile84 side chain. This same Ile84 rotamer preference is observed in the structures of the C-terminal macrocycles and bicycles (**5**−**7**) which, like **3**, have a small hydrophobic group at P2.

The macrocyclic components of **2** and **3** interact with the enzyme in the same manner as that described above for **1**, with the same hydrogen bonds forming between the enzyme and inhibitor. Inhibitor **3** has a valine in place of asparagine at P2 and therefore loses two hydrogen bonds but gains the van der Waals interaction with Ile84, compared with **1** and **2**. The loss of hydrogen bonds could explain the 10-fold lower K_i of **3** compared with that of **2**. The isostere hydroxyls of **2** and **3** are positioned almost exactly between the two catalytic aspartates (within hydrogen bonding distance of all four catalytic aspartate carboxylate oxygens). The conformation of the aromatic group in the macrocycle is constrained in the same way as in **1** ($\chi_1 \sim -40°$) so that van der Waals interactions with Gly49 and Ile50 are weaker than in the HIVPR−JG365 complex and interactions with other residues (Pro181 and Val182) are stronger. The equivalent angle for the aromatic P1 group in the acyclic VX-478 inhibitor is −52°, more like that observed for the acyclic JG365. As was found for **1**, the connecting trimethylene atoms of the N-terminal macrocycle in **2** and **3** are the least ordered of both inhibitors (Figure 1). The unfavorable contact between the macrocycle atom Cη_1 and Arg108 Nη_2 observed in the HIVPR−**1** complex is also present in these two structures.

The acyclic nonpeptidic sulfonamide regions of **2** and **3** interact with the enzyme in a similar manner. These interactions are also similar to those observed in the HIVPR−VX-478 complex (Figure 2). The electron density for the sulfonamide *N*-alkyl groups of both **2** and **3** suggests that this group is flexible when bound to the enzyme; two conformations were modeled in both enzyme complexes (Figure 1). The *N*-alkyl substituent interacts with the enzyme at the S1′ subsite. Hydrophobic interactions are formed with Pro81, Val82, and Val132. The sulfonamide phenyl ring binds in the enzyme S2′ subsite and interacts with Ile50, Ala128, Val132, and Ile147. One of the sulfonamide oxygens interacts with enzyme flap residues through Wat301, as is also observed in the crystal structure of the HIVPR−VX-478 complex.

The two bulky groups of **4** at P1′ (piperidine) and P2′ (*tert*-butyl) bring different constraints to the binding mode of the N-terminal macrocylic inhibitor. The conformation about the isostere region of **4** is like that of **2** and **3** rather than that of **1**. This is to be expected given that **4** has a large hydrophobic group at P1′, so the (*R*)-stereoisomer is preferred. The first two dihedral angles of **4** that define the isostere conformation are within 10° of the equivalent angles observed for **2** and **3**, but the third dihedral angle (see Table 3) differs by ∼50° from those of **2** and **3**. This is because the very bulky piperidine and *tert*-butyl groups of **4** impose a preference for a trans conformation at this point. Furthermore, the binding position of **4** in the enzyme active site is translated in the direction of its C-terminus by ∼0.5 Å compared with the other three N-terminal macrocycles (Figure 4). This translation apparently helps to optimize favorable contacts and minimize unfavorable interactions between the enzyme and the bulky *tert*-butyl group at P2′. Despite these conformational and binding adaptations, there is an unfavorable interaction observed in the crystal structure of the HIVKI−**4** complex between the C3 atom of the *tert*-butyl group and the main chain oxygen of Gly148 (3.4 Å). These findings

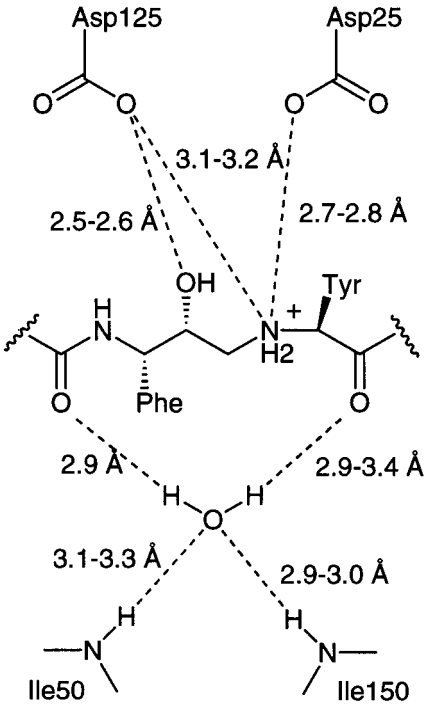

FIGURE 5: Representation of hydrogen bond interactions between the HIVPR active site, Wat301, and the scissile bond isostere of the C-terminal macrocycle (**5** and **6**) and bicycle (**7**). Note the interaction between the secondary amine of the inhibitor isostere and the HIVPR catalytic aspartates (Asp25 and Asp125).

suggest that a secondary rather than a tertiary alkyl substituent may be optimal at the P2′ position of HIVPR inhibitors if the P1′ group is also large and bulky.

A C-Terminal Macrocyclic Mimic for Phe-Ile-Val. Inhibitors **5** and **6** have the same C-terminal macrocycle derived through cyclization of phenylalanine and valine side chains of a C-terminal tripeptide, Phe-Ile-Val (Chart 1). They also have the same hydroxyethylamine transition state isostere that was used in the N-terminal macrocycle inhibitors. However, a major difference is that the nitrogen of the isostere in compounds **1**−**4** is a tertiary nitrogen (in proline or piperidine for **1** and **4**), but in the C-terminal macrocycles, it is a positively charged secondary amine nitrogen. As a consequence, there is an additional rotatable bond between the N-terminal P1 and C-terminal P1′ side chains compared with the previous macrocycles so that the bonds about this protonated nitrogen in **5** and **6** are less constrained than in the other inhibitors.

The high-resolution crystal structures of HIVKI complexed with the two C-terminal macrocyclic peptidomimetics show that the hydrogen bonds formed between the backbone atoms of JG365 or the N-terminal macrocycle inhibitors and HIVPR (Figure 3) are generally retained in the complexes with **5** and **6**. However, a significant difference occurs in the interaction with the hydroxyethylamine isostere (Figure 5). The hydroxyl groups of **1**−**4** are positioned between and can interact with both catalytic aspartates. For **5** and **6**, the hydroxyl of the isostere interacts with only one aspartate (Asp125) and the protonated secondary nitrogen interacts with the second aspartate (Asp25). To achieve this unusual interaction, the C-terminal macrocycle in **5** and **6** is translated in the active site in the direction of the inhibitor N-terminus by ∼1.5 Å compared with the bound position of N-terminal macrocyclic compounds **1**−**3** (Figure 4). This translation is in the direction opposite of that observed for **4**. Furthermore, the isostere dihedral angles of **5** and **6** are very different from those observed for **1**−**4** (Table 3) due to the additional flexibility in this region and, presumably, the need to optimize interactions of both the hydroxyl and the amine with the catalytic aspartates. As a consequence, the isostere hydroxyls of the N-terminal and C-terminal macrocyle inhibitors (**1**−**4** vs **5** and **6**) are separated by ∼2.5 Å in the enzyme active site (Figure 4).

The interaction between the protonated nitrogen of the C-terminal macrocycle inhibitors and the catalytic aspartate of HIVPR appears to be unique for inhibitors of HIVPR, though it has been proposed theoretically for an amino-diol isostere (*36*).

The quality of the electron density for ring atoms of the C-terminal macrocycles of both **5** and **6** is excellent (Figure 1). Furthermore, the *B*-factors for these atoms are similar to those of other inhibitor atoms. This suggests that these atoms are well-ordered in **5** and **6**, in contrast to the more flexible ring atoms in the N-terminal macrocycles.

The N-terminal component of inhibitors **5** and **6** retains the backbone hydrogen bond interactions described above for inhibitors **1**−**4**, but hydrophobic interactions with P1 and P2 side chains are weaker than those of **1**−**4** or JG365. The less sterically encumbered and protonated secondary amine of **5** and **6** allows strong ionic contact with the catalytic aspartates, and this presumably induces the translated fit of the inhibitor to the enzyme. However, the ionic interaction and inhibitor translation may be at the cost of weaker P1 and P2 hydrophobic interactions. There are no unfavorable interactions observed between atoms of the C-terminal macrocyle inhibitors and atoms of Arg8.

A Bicyclic Mimic for a Hexapeptide (Leu-Val-Phe-Phe-Ile-Val). The bicyclic inhibitor **7** consists of both an N-terminal and a C-terminal macrocycle, each corresponding to a tripeptide mimic. These two macrocyles are linked together by a hydroxyethylamine transition state isostere. The N-terminal macrocycle of **7** has a valine at the P2 position, similar to that of **3**, but there is an additional atom in the macrocycle compared with **1**−**4** (Chart 1). The C-terminal macrocycle and the transition state isostere of **7** are exactly the same as those of inhibitors **5** and **6**.

The question to be addressed was whether the bicyclic inhibitor would interact with the enzyme in the manner of the N-terminal or C-terminal macrocyle inhibitors. The crystal structure of the HIVKI−**7** complex shows that the bicyclic inhibitor binding mode has the same distinguishing features as the C-terminal macrocycles, consistent with the idea that the amine−aspartate interaction is the principal determinant of inhibitor location. A similar interaction occurs between the inhibitor-protonated secondary amine and enzyme catalytic aspartate; similar dihedral angles are observed for the isostere rotatable bonds (Table 3), and a similar translation of the inhibitor in the active site with respect to the N-terminal macrocycles is also evident (Figure 4). Also, the quality of the electron density is excellent for all atoms of the C-terminal macrocycle of **7**, and two conformations were modeled for the P2′ isoleucine side chain (Figure 1). However, electron density for the connecting trimethylene group of the N-terminal macrocyle is again poor (Figure 1), and two of these N-terminal macrocycle atoms were not modeled in the final refined structure.

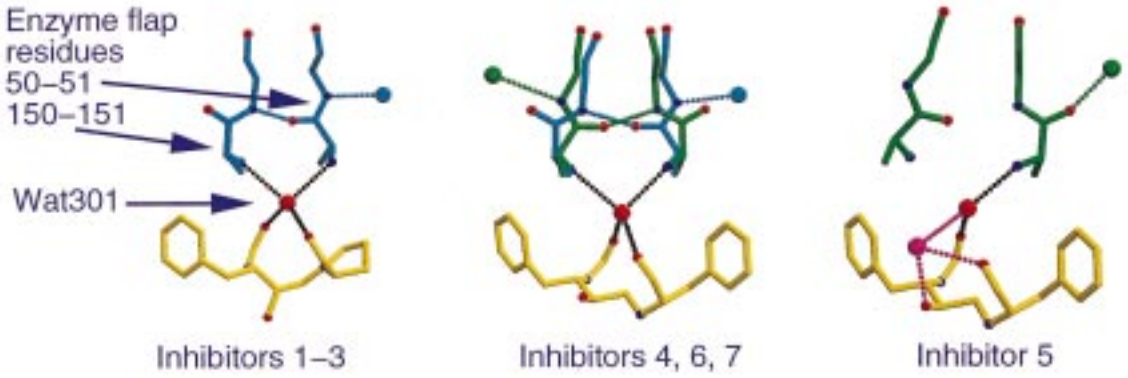

FIGURE 6: Disorder in HIVPR flap residues. Flap residues 50 and 51 and 150 and 151 are shown together with the bridging water, Wat301, and the central part of the macrocyclic inhibitor. Three different arrangements of the enzyme flap residues are observed in the crystal structures, shown here in the left, middle, and right panels. The conformation shown in the left panel (blue) is that most commonly observed in HIVPR−inhibitor crystal structures. In the middle panel, the flaps have two alternate conformations as observed in the enzyme complexes with **4**, **6**, and **7**. In the enzyme complex with **5** (right), an additional water (pink) interacts with the inhibitor near the flaps and interactions between Wat301, the inhibitor, and flap residues are weakened. A 3.3 Å distance cutoff was used to define hydrogen bonds (shown as dotted lines).

Interactions between Water and the HIVPR Flap Region. The two enzyme flaps that form part of the inhibitor-binding site can adopt open (uncomplexed) or closed (bound) conformations. In crystal structures of the open HIVPR form (*7*, *8*), the two flaps adopt identical (symmetry-related) conformations. Upon the binding of a peptidic inhibitor, there is a conformational change and the bound flap conformations become nonidentical (*9*). Crystal structures of the closed HIVPR conformation show that a water (Wat301) mediates interactions between the bound inhibitor and flap residues (Ile50 and Ile150) of the enzyme through formation of four tetrahedrally coordinated hydrogen bonds (*9*). This change in the conformation of the HIVPR flaps upon binding inhibitors is thought to be critical for catalytic function.

In several of the crystal structures described here, two alternate conformations (static disorder) are observed for the backbone amide of flap residues Ile50 and Gly51 and Ile150 and Gly151 (Figure 6). A weaker interaction with Wat301 appears to accompany the static disorder of the flap residues. For example, in the structures of the three complexes where there is no evidence for static disorder of the flap residues (N-terminal macrocycles **1**−**3**), Wat301 makes the usual strong hydrogen bond interactions with surrounding tetrahedrally arranged inhibitor carbonyl oxygens (2.7−2.8 Å) and amide nitrogens of enzyme residues Ile50 and Ile150 (2.8−3.0 Å). The *B*-factor of Wat301 in these three structures is low (7−12 Å^2), suggesting that it is bound tightly in the complex. Crystal structures of HIVKI complexed with the N-terminal macrocycle **4** or the C-terminal macrocycle **6** incorporate the flap residues modeled with two alternate backbone conformations. In these two structures, Wat301 has a higher *B*-factor (15−17 Å^2) and the hydrogen bond distances to the inhibitor carbonyl oxygens (2.9−3.0 Å) and to the flap amide nitrogens (2.9−3.1 Å) are lengthened. The crystal structure of HIVKI complexed with the bicycle **7** exhibits this same static disorder of the flap residues and lengthened hydrogen bond distances to Wat301. However, the *B*-factor of Wat301 in the HIVKI−**7** structure (11 Å^2) suggests that it is well-ordered.

In the HIVKI−**5** complex, the geometry in this region is different again. A single backbone conformation is present for the flap region, but the peptide conformations of Ile50 and Gly51 and Ile150 and Gly151 are inverted (Figure 6) compared to those found in most HIVPR complexes (and compared with those observed in complexes with **1**−**3**). The usual hydrogen bond interaction between the peptide bond of Ile50 and Gly51 and the peptide bond of Ile150 and Gly151 is lost (>3.3 Å). The flap of residues 48−52 is in a more open conformation in the HIVKI−**5** complex (the distance between Ile50 Cα and Asp125 Cα is 13.2 Å compared with 12.4−13.0 Å for the other six crystal structures), while the flap of residues 148−152 is in a more closed conformation than usual (distance between Ile150 Cα and Asp25 Cα is 12.1 Å compared with 12.3−12.8 Å for the other six). Furthermore, hydrogen bond distances to Wat301 (*B*-factor of 22 Å^2) are lengthened in the HIVKI−**5** complex so that only two of the usual four hydrogen bond interactions are formed (using a 3.3 Å distance cutoff for hydrogen bonds); interactions with one of the flap amide nitrogens and one of the inhibitor carbonyl oxygens are lost. Instead, this inhibitor carbonyl oxygen interacts with another water (3.0 Å) (pink in Figure 6) that also forms hydrogen bonds with the hydroxyl group of the inhibitor isostere (2.6 Å) and with Wat301 (3.1 Å). This water (*B*-factor of ∼30 Å^2) is not observed in the other six HIVPR/KI−macrocyclic inhibitor structures reported here and may be present in HIVKI−**5** because of the slightly more open conformation of the enzyme flap (residues 48−52).

DISCUSSION

A number of key results have emerged from this work, including the advantages of using a mutant enzyme in crystallography studies, the remarkable ability of cyclic compounds to structurally and functionally mimic peptide inhibitors of a protease, the importance and structural influence of charged interactions in the active site of the protease, and the disorder and flexibility of HIVPR flap residues.

HIVKI in Crystallography. HIVKI has important advantages over HIVPR in crystallization work in that it is significantly more stable to autolysis because the autocleavage sites of HIVPR are mutated (Gln7Lys and Leu33Ile). Preventing self-degradation through removal of these autocleavage sites not only maximizes the enzyme concentration

for inhibitor binding but also prevents formation of self-degradation peptides that can compete as inhibitors for binding to the enzyme active site. The structures of **2**−**7** reported here were determined from cocrystals with HIVKI, while the cocrystal of **1** was derived from HIVPR. The structures of the HIVKI and HIVPR enzymes in these seven crystal structures are equivalent, within coordinate error. This result implies that HIVKI could be a useful alternative to HIVPR in experiments where autocleavage can be a problem.

Improved HIVPR Inhibitors. The crystal structures of complexes with **1**−**7** show that the macrocyclic component of the inhibitors mimics very well the binding mode of acyclic peptidic inhibitors. However, macrocyclic peptide inhibitors are also much more stable than acyclic peptide inhibitors because they are less susceptible to proteolysis (*15*). Furthermore, there is an entropic advantage in using a peptidic macrocycle since it is conformationally pre-organized for receptor binding compared with the acyclic peptide. Peptide inhibitors are reportedly (*1*) difficult to optimize because the local structure of both the enzyme and the inhibitor can be influenced by each other as well as by more remote conformational changes. The results reported here show that the macrocycle can be used in a modular fashion as a template, in combination with peptidic or nonpeptidic portions of other HIVPR inhibitors, without significantly altering the binding location or mode of interactions. A corollary to this is that a charged group in the inhibitor can apparently override these interactions and dictate the final position of each macrocycle as illustrated by results herein.

The unusual interaction observed between the protonated secondary amines of inhibitors **5**−**7** and the HIVPR catalytic aspartate opens up new possibilities for the design of novel HIVPR inhibitors. In particular, it shows how additional interactions can be made in the active site and how charged interactions can influence structure. The results also suggest that better combinations of charged interactions, hydrogen bonds, and hydrophobic effects are likely to lead to inhibitors with an affinity for HIVPR even higher than those of the inhibitors described here. Within the macrocycle class of inhibitors, it should be possible to analyze the contributions to inhibitor affinity of charged amines by (i) replacing the tertiary nitrogen from the N-terminal macrocycle isostere with a secondary amine nitrogen, (ii) replacing the secondary amine nitrogen from the C-terminal macrocycle isostere with a tertiary nitrogen, and (iii) replacing the secondary amine nitrogen from the C-terminal macrocycle isostere with a methylene group.

Implications for HIVPR Function and Inhibitor Design. An important finding from several structures of the macrocycle inhibitor complexes reported here was the observation of static disorder and flexibility in the region of the enzyme flaps. The dual conformations of the Ile50-Gly51 and Ile150-Gly151 regions of the enzyme are best described as a ∼180° flip of these peptide bonds. A similar peptide flip was observed in solution by NMR for a HIVPR complex with the cyclic urea inhibitor DMP323 (*37*) and in the crystal structure of a substrate complex of D30N feline immunodeficiency virus protease (*38*). Furthermore, in crystal structures of HIV-1 PR and HIV-2 PR inhibitor complexes (*39*, *40*), an increased distance between the enzyme flaps and bound inhibitor was accompanied by weaker binding of the flap water (Wat301) and increased flexibility of the flap residues.

In our work, the flap disorder appears to be correlated with a "translation" of the inhibitor in the active site, either toward the P1′, C-terminal end of the inhibitor (**4**, with bulky P1′ and P2′ groups) or toward the P1, N-terminal end of the inhibitor (**5**−**7**, with protonated secondary amine binding to the catalytic aspartates). The observed changes in the flap region of the enzyme may therefore resemble the changes that occur during the catalytic cycle where the two products derived from the substrate move apart in the active site. Separation of the cleavage products (or translation of the inhibitor in the active site) could be the trigger for opening of the flaps and release of product by disrupting hydrophobic interactions and weakening the interaction with Wat301.

Presumably, it would be important to minimize flap flexibility to optimize inhibitor binding to HIVPR. The flexibility of the flap residues in the enzymes bound with **4**−**7** may contribute to the reduced potency of these inhibitors compared with **2**, for example. Now that the binding of these inhibitors is known, it may be possible to design improved HIVPR inhibitors that have a charged group for binding to the catalytic aspartate without causing a translation of the inhibitor in the active site.

ACKNOWLEDGMENT

We thank Alun Jones (mass spectrometry) and Trudy Bond (amino acid analysis) for technical assistance.

REFERENCES

1. Tomasselli, A. G., Howe, W. J., Sawyer, T. K., Wlodawer, A., and Heinrikson, R. L. (1991) *Chim. Oggi 9*, 6−27.
2. Darke, P. L., and Huff, J. R. (1994) *Adv. Pharmacol. 25*, 399−454.
3. West, M. L., and Fairlie, D. P. (1995) *Trends Pharmacol. Sci. 16*, 67−75.
4. Kohl, N. E., Emini, E. A., Schleif, W. A., Davis, L. J., Meimbach, J. C., Dixon, R. A. F., Scolnick, E. M., and Sigal, I. S. (1988) *Proc. Natl. Acad. Sci. U.S.A. 85*, 4686−4690.
5. Ashorn, P., McQuade, T. J., Thaisrivongs, S., Tomasselli, A. G., Tarpley, W. G., and Moss, B. (1990) *Proc. Natl. Acad. Sci. U.S.A. 87*, 7472−7476.
6. McQuade, T. J., Tomasselli, A. G., Liu, L., Karacostas, V., Moss, B., Sawyer, T. K., Heinrikson, R. L., and Ratpley, W. G. (1990) *Science 247*, 454−456.
7. Wlodawer, A., Miller, M., Jaskolski, M., Sathyanarayana, B. K., Baldwin, E., Weber, I. T., Selk, L. M., Clawson, L., Schneider, J., and Kent, S. B. H. (1989) *Science 245*, 616−621.
8. Navia, M. A., Fitzgerald, P. M. D., McKeever, B. M., Leu, C.-T., Heimbach, J. C., Herber, W. K., Sigal, I. S., Darke, P. L., and Springer, J. P. (1989) *Nature 337*, 615−620.
9. Miller, M., Schneider, J., Sathyanarayana, B. K., Toth, M. V., Marshall, G. R., Clawson, L., Selk, L., Kent, S. B. H., and Wlodawer, A. (1989) *Science 246*, 1149−1152.
10. Wlodawer, A. (1994) *Pharmacotherapy 14*, 9S−20S.
11. Abdel-Meguid, S. S. (1993) *Med. Res. Rev. 13*, 731−778.
12. March, D. R., and Fairlie, D. P. (1996) in *Designing new antiviral drugs for AIDS: HIV-1 protease and its inhibitors* (Landes, R. G., Ed.) Springer-Verlag, Austin, TX.
13. Bernstein, F. C., Koetzle, T. F., Williams, G. J. B., Meyer, E. F., Jr., Brice, M. D., Rodgers, J. R., Kennard, O., Shimanouchi, T., and Tasumi, M. (1977) *J. Mol. Biol. 112*, 535−542.
14. Vondrasek, J., van Buskirk, C. P., and Wlodawer, A. (1997) *Nat. Struct. Biol. 4*, 8.
15. Reid, R. C., and Fairlie, D. P. (1997) *Adv. Amino Acid Mimetics Peptidomimetics 1*, 77−107.

16. Abbenante, G., March, D. R., Bergman, D. A., Hunt, P. A., Garnham, B., Dancer, R. J., Martin, J. L., and Fairlie, D. P. (1995) *J. Am. Chem. Soc. 117*, 10220−10226.
17. March, D. R., Abbenante, G., Bergman, D. A., Brinkworth, R. I., Wickramasinghe, W., Begun, J., Martin, J. L., and Fairlie, D. P. (1996) *J. Am. Chem. Soc. 118*, 3375−3379.
18. Schneider, J., and Kent, S. B. H. (1988) *Cell 54*, 363−368.
19. Bergman, D. A., Alewood, D., Alewood, P. F., Andrews, J. L., Brinkworth, R. I., Englebretsen, D. R., and Kent, S. B. H. (1995) *Lett. Pept. Sci. 2*, 99−107.
20. Rose, J. R., Salto, R., and Craik, C. S. (1993) *J. Biol. Chem. 268*, 11939−11945.
21. Mildner, A. M., Rothrock, D. J., Leone, J. W., Bannow, C. A., Lull, J. M., Reardon, I. M., Sarcich, J. L., Howe, W. J., Tomich, C.-S. C., Smith, C. W., Heinrikson, R. L., and Tomasselli, A. G. (1994) *Biochemistry 33*, 9405−9413.
22. Hui, J. O., Tomasselli, A. G., Reardon, I. M., Lull, J. M., Brunner, D. P., Tomich, C.-S. C., and Heinrikson, R. L. (1993) *J. Protein Chem. 12*, 323−327.
23. Toth, M., and Marshall, G. R. (1990) *Int. J. Pept. Protein Res. 36*, 544−550.
24. Otwinowski, Z., and Minor, W. (1997) *Methods Enzymol. 276*, 307−326.
25. Swain, A. L., Miller, M. M., Green, J., Rich, D. H., Schneider, J., Kent, S. B. H., and Wlodawer, A. (1990) *Proc. Natl. Acad. Sci. U.S.A. 87*, 8805−8809.
26. Brünger, A. T. (1992) *X-PLOR (Version 3.1) Manual*, Yale University Press, New Haven, CT.
27. Brünger, A. T. (1993) *Acta Crystallogr. D49*, 24−36.
28. Jones, T. A., Zou, J. Y., Cowan, S. W., and Kjeldgaard, M. (1991) *Acta Crystallogr. A47*, 110−119.
29. Engh, R. A., and Huber, R. (1991) *Acta Crystallogr. A47*, 392−400.
30. Evans, S. V. (1993) *J. Mol. Graphics 11*, 134−138.
31. Kraulis, P. J. (1991) *J. Appl. Crystallogr. 24*, 946−950.
32. Bacon, D. J., and Anderson, W. F. (1988) *J. Mol. Graphics 6*, 219−222.
33. Merritt, E. A., and Murphy, M. E. P. (1994) *Acta Crystallogr. D50*, 869−873.
34. Roberts, N. A., Craig, J. C., and Duncan, I. B. (1992) *Biochem. Soc. Trans. 20*, 513−516.
35. Kim, E. E., Baker, C. T., Dwyer, M. D., Murcko, M. A., Rao, B. G., Tung, R. D., and Navia, M. A. (1995) *J. Am. Chem. Soc. 117*, 1181−1182.
36. Bisacchi, G. S., Ahmad, S., Alam, M., Ashfaq, A., Barrish, J., Cheng, P. T. W., Greytok, J., Hermsmeier, M., Lin, P.-F., Merchant, Z., Skoog, M., Spergel, S., and Zahler, R. (1995) *Bioorg. Med. Chem. 5*, 459−464.
37. Nicholson, L. K., Yamazaki, T., Torchia, D. A., Grzesiek, S., Bax, A., Stahl, S. J., Kaufman, J. D., Wingfield, P. T., Lam, P. Y. S., Jadhav, P. K., Hodge, C. N., Domaille, P. J., and Chang, C.-H. (1995) *Struct. Biol. 2*, 274−279.
38. Laco, G. S., Schalk-Hihi, C., Lubkowski, J., Morris, G., Zdanov, A., Olson, A., Elder, J. H., Wlodawer, A., and Gutschina, A. (1997) *Biochemistry 36*, 10696−10708.
39. Lange-Savage, G., Berchtold, H., Liesum, A., Budt, K. H., Peyman, A., Knolle, J., Sedlacek, J., Fabry, M., and Hilgenfeld, R. (1997) *Eur. J. Biochem. 248*, 313−322.
40. Mulichak, A. M., Hui, J. O., Tomasselli, A. G., Heinrikson, R. L., Curry, K. A., Tomich, C.-S., Thaisrivongs, S., Sawyer, T. K., and Watenpaugh, K. D. (1993) *J. Biol. Chem. 268*, 13103−13109.

BI990174X